The Journal of Clinical Pharmacology
2021, 61(9) 1232–1242

DOI: 10.1002/jcph.1876

Longitudinal Impact of Acute Spinal Cord Injury on Clinical Pharmacokinetics of Riluzole, a Potential Neuroprotective Agent

Ashley Nguyen, PhD[1], Diana S-L. Chow, PhD[1], Lei Wu, PhD[1], Yang (Angela) Teng, PhD[1,2], Mahua Sarkar, PhD[1], Elizabeth G. Toups, MSc[3], James S. Harrop, MD[4], Karl M. Schmitt, MD[5], Michele M. Johnson, MD[5,6], James D. Guest, MD, PhD[7], Bizhan Aarabi, MD[8], Christopher I. Shaffrey, MD[9,10], Maxwell Boakye, MD[11], Ralph F. Frankowski, PhD[12], Michael G. Fehlings, MD, PhD[13], and Robert G. Grossman, MD[3]

Abstract

Riluzole, a benzothiazole sodium channel blocker that received US Food and Drug Administration approval to attenuate neurodegeneration in amyotrophic lateral sclerosis in 1995, was found to be safe and potentially efficacious in a spinal cord injury (SCI) population, as evident in a phase I clinical trial. The acute and progressive nature of traumatic SCI and the complexity of secondary injury processes can alter the pharmacokinetics of therapeutics. A 1-compartment with first-order elimination population pharmacokinetic model for riluzole incorporating time-dependent clearance and volume of distribution was developed from combined data of the phase I and the ongoing phase 2/3 trials. This change in therapeutic exposure may lead to a biased estimate of the exposure-response relationship when evaluating therapeutic effects. With the developed model, a rational, optimal dosing scheme can be designed with time-dependent modification that preserves the required therapeutic exposure of riluzole.

Keywords

pharmacokinetics, population modeling, riluzole, spinal cord injury

Spinal cord injury (SCI) impairs physical and psychological health, independence, and quality of life of patients. Approximately 17 810 new cases of SCI are reported every year, and currently between 250 000 and 368 000 people are chronically affected by SCI in North America alone.[1]

Establishing effective therapies for patients with SCI is an ongoing effort. Currently, a leading candidate to improve neurological outcomes following traumatic injury, based on initial clinical studies, is riluzole.[2] It is a US Food and Drug Administration (FDA)–approved drug for amyotrophic lateral sclerosis (ALS).[3,4]

[1]Department of Pharmacological and Pharmaceutical Sciences, College of Pharmacy, University of Houston, Houston, Texas, USA
[2]Covance, Madison, Wisconsin, USA
[3]Department of Neurosurgery, Houston Methodist Research Institute, Houston, Texas, USA
[4]Department of Neurosurgery, Thomas Jefferson University, Philadelphia, Pennsylvania, USA
[5]Department of Neurosurgery, Health Science Center, University of Texas, Houston, Texas, USA
[6]Atlanta Brain and Spine Care, Atlanta, Georgia, USA
[7]Department of Neurological Surgery, Miller School of Medicine, University of Miami, Miami, Florida, USA
[8]Department of Neurosurgery, University of Maryland, Baltimore, Maryland, USA
[9]Department of Neurosurgery, University of Virginia Health System, Charlottesville, Virginia, USA
[10]Department of Neurosurgery, Duke University Medical Center, Durham, North Carolina, USA
[11]Department of Neurosurgery, University of Louisville, Louisville, Kentucky, USA
[12]Late colleague, Division of Biostatistics, University of Texas School of Public Health, Houston, Texas, USA
[13]Division of Neurosurgery and Spine Program, Toronto Western Hospital, University of, Toronto, Ontario, Canada

Submitted for publication 13 January 2021; accepted 18 April 2021.

Corresponding Author:
Ashley Nguyen, PhD, University of Houston College of Pharmacy, Department of Pharmacological and Pharmaceutical Sciences, 4849 Calhoun Road, Health Building 2, Room 7051, Houston, TX 77204
Email: nguyenashley89@gmail.com

Riluzole, a benzothiazole anticonvulsant sodium channel blocker, has the potential to protect nerve cells and promote functional neurological recovery after physical injury.[5,6] Neuroprotective mechanism attenuates secondary injury cascade by maintaining neuronal ionic balance and inhibiting excitotoxic glutamate release. Preclinical studies using a rodent SCI model have demonstrated the association between riluzole treatment and reduced neurological tissue destruction at the injury site, thus improving functional outcomes. Riluzole is an oral tablet that is well absorbed from the gastrointestinal tract with absolute bioavailability of approximately 60%. A high-fat meal significantly reduces the bioavailability of the drug by prolonging absorption. Despite large interindividual variability, riluzole plasma concentrations are linearly related to the administered dose over dose ranges of 25-250 mg.[7] Riluzole is extensively metabolized in the liver by cytochrome P450 (CYP1) A1/2, followed by glucuronide conjugation to be eliminated renally, with only 0.5% of dose excreted unchanged.[7] Having an intermediate extraction ratio and high plasma protein binding (96%), riluzole plasma concentration is influenced by blood flow, intrinsic clearance, and fraction unbound. The drug distributes extensively into the tissues and have been shown to cross the blood-brain/spinal cord barrier. Preclinical and clinical data obtained after repeated dosing do not suggest any autoinduction or autoinhibition capability of riluzole on CYP1A1/2 enzymes.

It is important to understand how traumatic SCI uniquely affects drug levels to optimize the treatment protocols. A successful phase 1 clinical trial indicated that riluzole taken orally is well tolerated and potentially efficacious in improving neurological outcomes of traumatic cervical SCI patients. However, the progressive nature of SCI pathology leads to altered pharmacokinetics (PK) of the orally delivered riluzole during the treatment course of 14 days. The phase 1 PK study documented the riluzole PK changes showing a significantly higher peak concentration (C_{peak}), trough concentration (C_{trough}), and 12-hour exposure ($AUC_{0\rightarrow12}$) on day 3 post–drug initiation than on day 14, a robust phenomenon consistently observed in all patients at all clinical sites.[8] PK analysis revealed that these changes resulted from higher clearance (CL/F) and larger volume of distribution (V_d/F) on day 14 compared with those on day 3. Lower exposure of riluzole on the same dose basis at the later stage of treatment can limit treatment efficacy. Therefore, it is imperative to quantitatively characterize the trend in PK changes and understand the potential impacts of those changes on the overall neurologic recovery, functional outcomes, mortality, and adverse events. A multicenter randomized, placebo-controlled, double-blind Riluzole in Acute Spinal Cord Injury Study (RISCIS) phase 2/3 trial is currently ongoing, in which a PK substudy is performed to characterize the dynamic PK changes that take place between day 3 and day 14 of the treatment.[9] In this article, information gained from PK studies of both phase 1 and partially accomplished phase 2/3 are used to develop a population pharmacokinetic model that can describe the time-varying parameters induced by SCI progression. The resulting validated population pharmacokinetic model can be used to guide rational dosing to maintain the therapeutic exposure of riluzole treatment throughout the course of 2 weeks, despite the heterogeneous nature of injury in the population and the complex cotreatments for secondary adverse events.

Methods

SCI Patient Demographics

The concentration-time data used for analysis were collected from 2 clinical trials, both of which received ethical institutional review board approval from the individual participating institutions. Informed consent was obtained from all patients. The phase 1 clinical trial investigating the safety and pharmacokinetics of riluzole was completed in 2011 (ClinicalTrials.gov Identifier: NCT00876889). RISCIS (ClinicalTrials.gov Identifier: NCT01597518) is presently an ongoing phase 2/3 multicenter randomized, placebo-controlled, double-blind trial to evaluate efficacy and safety of riluzole in the treatment of patients with acute SCI. The sites funded by the Department of Defense received Human Research Protection Office approval. The protocols that followed were in compliance with Good Clinical Practices.

The phase 1 trial recruited 36 patients with these inclusion criteria: age from 18 to 70 years; American Spinal Injury Association impairment scale grades A, B, or C; able to receive the drug within 12 hours of injury; written informed consent; and traumatic SCI injury level between C4 and T12. The subsequent phase 2/3 trial has recruited 146 patients for inclusion in this study, with 31 patients enrolled in this sub-PK study. Inclusion criteria for phase 2/3 were similar to those of phase 1, except for SCI injury level between C4 and C8. The exclusion criteria for both studies included hypersensitivity to riluzole; penetrating injury; concomitant head injury, defined as Glasgow Coma Scale score < 14; preexisting neurologic or mental disorder; history of chemical substance dependence; liver or kidney disease; pregnancy; prisoner; and participation in another clinical trial. In total, 227 riluzole plasma concentrations from 47 patients (34 from phase 1 and 13 from phase 2/3) were used in this analysis. The medication log for each patient was obtained to screen for potential concomitant drug-drug interactions.

Riluzole Treatment and Blood Sampling Protocol

Phase 1 participants received a 50-mg dose every 12 hours for 14 days. The dose was selected based on a randomized, controlled trial of riluzole in patients with ALS, in which the efficacy and safety of riluzole in twice-daily doses of 25, 50, and 100 mg were investigated. The dose of 50 mg twice daily was selected because the dose of 25 mg offers insignificant merit over placebo; doses of 50 and 100 mg are superior to placebo, with no difference between the 2 doses, but the dose of 50 mg twice daily had the best benefit/harm ratio.[4] In this phase 1 study, plasma samples were collected 1 hour predose and within 1-2 hours postdose on the third and 14th days.

Phase 2/3 participants received a 100-mg loading dose every 12 hours on the first day, followed by a 50-mg dose every 12 hours for the remaining 13 days of the treatment. To supplement the observation of variant PK from the phase 1 study, additional samples on days 7 and 10 were collected. Specifically, plasma sampling was performed immediately before dose, and approximately 3 hours postdose on days 3, 7, 10, and 14.[8] Recognizing different sampling times between the 2 studies, actual dosing and sampling times for each study were recorded and applied in our data file.

Riluzole was taken at least an hour before or 2 hours after, a meal to avoid a food-related decrease in bioavailability. SCI patients often experience injury-related complications that require administration of several concomitant medications. Only noncontraindicated concomitant medications were administered and recorded.

Liquid Chromatography-Tandem Mass Spectrometry Quantification

Riluzole concentrations were quantified using an liquid chromatography-tandem mass spectrometry assay method previously developed and validated.[10] Riluzole and its radiolabeled internal standard (IS) [^{13}C,$^{15}N_2$] riluzole were isolated from plasma by liquid-liquid extraction using ethyl acetate. Riluzole and IS elution at 1.9 minutes was achieved using 0.4 mL/min isocratic flow through a Waters AQUITY UPLC BEH C18 column (2.1 × 50 mm, 1.7-μm particle size) with the mobile phase composed of 20% ACN and 80% MeOH:water (70:30, v/v) containing 0.1% formic acid. Riluzole (m/z 235 → 166) and IS (m/z 238 → 169) were detected by electrospray ionization using multiple reaction monitoring in a positive mode on a QTRAP 3200 System (AB SCIEX, Framingham, Massachusetts). The assay had linearity established between 0.5 (the lower limit of quantitation) and 800 ng/mL and intraday and interday accuracy and precision of riluzole assay within 10%, meeting the requirements of FDA guidelines.

PK Data Analysis

PK analysis was executed in Phoenix NLME, version 8.2 (Certara L.P. Pharsight, St. Louis, Missouri). The population analysis of phase 1 data provided reasonable initial estimates and structural modeling for the final model, which included both phase 1 and phase 2/3 data.[8] Although the PK parameters were estimated using only 2 concentration-time data on each sampling day, potentially limiting the structural model to having only 1 compartment, the model generated can still serve our purpose of describing the dynamic PK changes that took place throughout the 14-day treatment period. A naive-pooled method was used to confirm the initial estimates and structural model using Akaike information criterion (AIC), an extension of the minus twice the log likelihood, as the selection criterion. AIC differences of $\geq$4 were regarded as significant. Nonlinear mixed-effects modeling was performed using the first-order conditional estimation–extended least-squares (FOCE-ELS) approach to generate the model. The interpatient variability of estimated parameters was assumed to follow a normal distribution, with a mean of 0 and variance of ω^2. Residual variability, referring to unexplained intrapatient variability, experimental error, and model misspecification, was estimated using additive, multiplicative, and combined residual models, respectively.

Model selection was informed by evaluating goodness-of-fit criteria, including AIC, precision, and scientific plausibility of parameter estimates and visual inspection of graphical goodness-of-fit plots. Internal validation was performed by nonparametric bootstrapping without stratification (n = 1000).

One-compartment models incorporating empirical equations for time-varying CL and V were explored to describe the change in the PK of riluzole over the 2-week period of treatment. Several approaches to capturing the time-dependent components of CL and V_d have been discussed in the literature to characterize the PK of several antibodies for anticancer immunotherapies.[11–13] Liu et al modeled the decrease in CL of nivolumab, human PD-1 blocking antibody, as a sigmoidal maximal inhibitory response process.[11] The same approach was used by Wilkins et al to explain the time-dependent increase in CL of avelumab, human anti-PD-L1 antibody.[12] Gibiansky's time-varying CL model for obinutuzumab, humanized anti-CD20 monoclonal antibody, included parallel time-independent and time-dependent CL processes.[13] However, these approaches did not support the model fitting for our data. Our PK study was designed to capture the trends in which clearance and volume of distribution were changing throughout the treatment period and thus only had 2 concentration-time data per dose. The time-varying models previously described

in the literature were made possible by having frequent sample collections that enabled complex parameterization. Moreover, these suggested models were developed to describe large molecules, which behave differently in terms of mechanism and PK fate.[14] Very few publications described small molecules exhibiting time-variant PK. One of these publications comprehensively discussed several mathematical models, including linear, exponential, concave, sigmoidal E_{max}, and Weibull functions to characterize the increase in elimination over time of polyethylene glycol (PEG)–conjugated asparaginase oncaspar.[15] The authors found that sigmoidal E_{max} and Weibull models with clearance as a function of time after dose, rather than time after first administration, best described the time dependence of PEG-ASNase. This suggested that drug-related effects were predominantly driving the increase in elimination of Oncaspar. The PK of riluzole, however, is clearly affected by pathophysiological changes as a result of injury and therefore would be best characterized by a function of time after the initial dose that eventually plateaus, as the nature of all biological processes. Consequently, the final riluzole model was built using a simplified version of Wilkins's approach to describe the time-dependent increase in parameters observed in our data, using Michaelis Menten kinetics as illustrated in equation 1:

$$PAR_{i,t} = tvPAR \times \exp\left(\frac{I_{\max,i} \times Time_i}{t_{50,i} + Time_i}\right) \times \exp(\eta PAR_i) \quad (1)$$

where $PAR_{i,t}$ is the parameter value of individual i at time t, $tvPAR$ is the typical values of PK parameters for the population, $I_{max,i}$ is the maximal fold-change of that parameter relative to baseline, $Time_i$ is the time after the first dose in individual i, t_{50i} indicates the time at which 50% of I_{max} is reached, and ηPAR_i is interpatient variability in the parameter estimate for individual i.

We performed visual predictive checks at each individual development step leading to the final model. Concentration-time profiles were simulated 1000 times using the corresponding dosing regimen for phase 1 and phase 2/3 patients. The prediction intervals at 5%, 50%, and 95% quantiles obtained from the simulation were compared and plotted against the observation intervals. The predictive performance of the model was evaluated based on the capability of prediction intervals to encompass original observations.

Results

Base Population PK Model

Riluzole concentrations in SCI patients were presented in waterfall plots on days 3 (n = 34) and 14 (n = 31) from phase 1 and on days 3 (n = 13), 7 (n = 13), 10 (n = 13), and 14 (n = 12) from phase 2/3 (Figure 1). In phase 1, day 3 concentrations were higher than day 14 concentrations, with higher ranges (8.7-126 vs 2.9-46.0 ng/mL for C_{trough}; 21.5-270 vs 12.4-154.5 ng/mL for C_{peak}) and higher medians (37.2 vs 16.2 ng/mL for C_{trough}; 87 vs 51.6 ng/mL for C_{peak}). In phase 2/3, the same trend was observed, with day 3

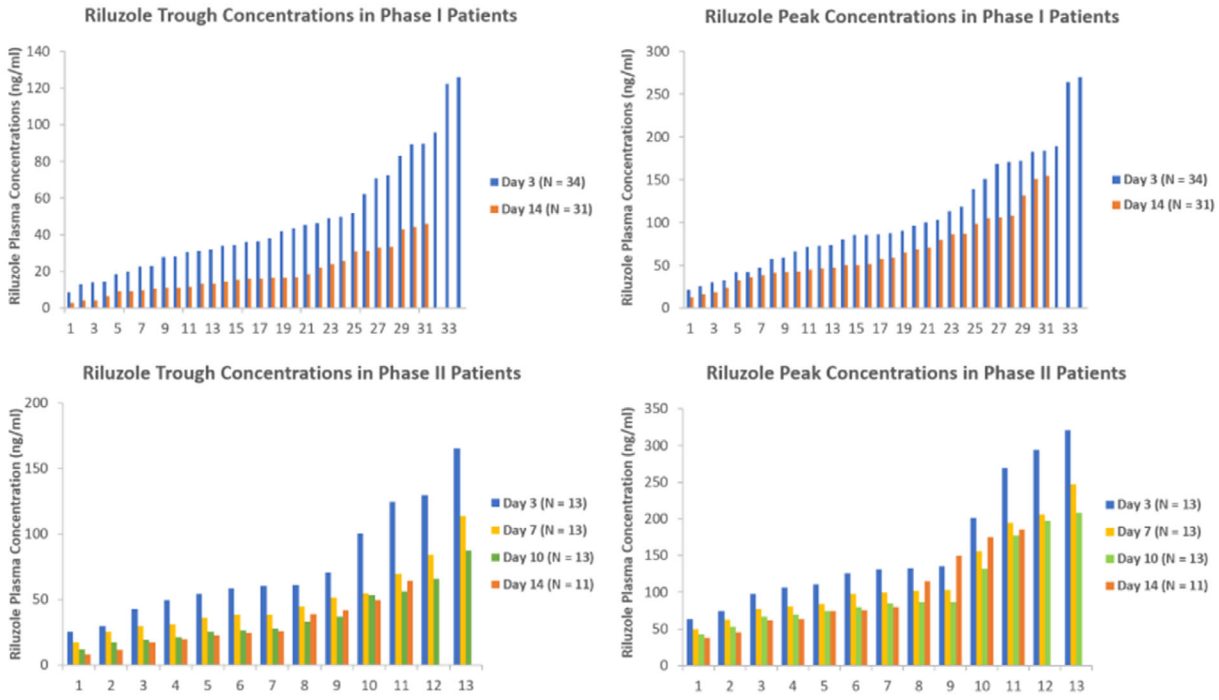

Figure 1. Riluzole concentrations presented in low-high order on days 3, 7, 10, and 14.

Table 1. Summary of Riluzole Concentrations From Phase 1 and Phase 2/3 Trials

Study	Parameters	Statistics	Day 3	Day 7	Day 10	Day 14
Phase 1	C_{trough}	Median (ng/mL)	37.2			16.2
		Range (ng/mL)	8.7-126.0			2.9-46.0
	C_{peak}	Median (ng/mL)	87.0			51.6
		Range (ng/mL)	21.5-270.0			12.4-154.5
Phase 2/3	C_{trough}	Median (ng/mL)	60.6	48.9	27.8	25.3
		Range (ng/mL)	25.7-165.0	17.3-113.9	11.9-87.5	8.3-64.3
	C_{peak}	Median (ng/mL)	130.8	99.1	84.9	77.7
		Range (ng/mL)	63.7-320.8	49.7-247.4	42.8-208.4	37.6-185.4

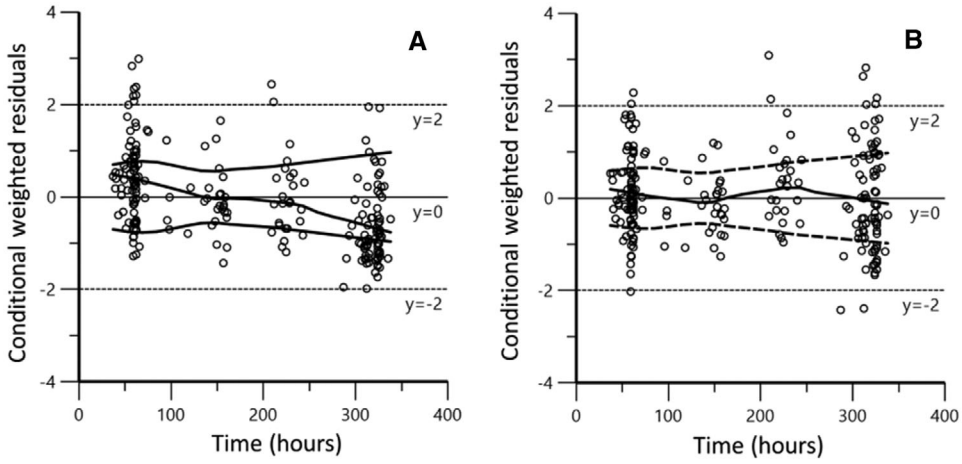

Figure 2. Comparison between diagnostic CWRES-IVAR plots for base model (A) versus final model (B).

having higher ranges (25.7-165.0 vs 8.3-64.3 ng/mL for C_{trough}; 63.7-320.8 vs 37.6-185.4 ng/mL for C_{peak}) and higher medians (60.6 vs 25.3 ng/mL for C_{trough}; 130.8 vs 77.7 ng/mL for C_{peak}) than those on day 14 (Table 1). The observation confirmed the time-varying PK of riluzole in the SCI population previously documented in a phase 1 clinical trial.[8]

This phase 1 study revealed that the C_{max} and $AUC_{0\text{-}12}$ achieved in SCI patients were lower than those in ALS patients on the same dose basis, particularly because of a higher CL/F and larger V_d/F.[8] The report applied individual and population PK analysis on day 3 and day 14 separately and concluded that C_{max}, C_{min}, and $AUC_{0\text{-}12}$ (128.9 ng/mL, 45.6 ng/mL, and 982.0 ng·h/mL, respectively) were significantly higher on day 3 than on day 14 (76.5 ng/mL, 19.1 ng/mL, and 521.0 ng·h/mL, respectively).[8] CL/F was lower (49.5 vs 106.2 L/h) and V_d/F (557.1 vs 1297.9 L) was smaller on day 3 compared with those on day 14.[8]

The parameter estimates derived from this study were used as initial estimates for the base model combining phase 1 and phase 2/3 data that included observations from day 7 and day 10 in addition to the original sampling scheme on day 3 and day 14 after the first dose. The base model was a time-stationary 1-compartment model without a time-dependent factor. The plot of conditional weighted residual (CWRES)–independent variable (IVAR), time after the first dose for the base model indicated an overestimation of the observed riluzole concentrations toward later times, suggesting that a time-varying PK property of riluzole in this population was not adequately captured by the time-stationary model (Figure 2A).

Time-Varying PK Model

The addition of the time-postinjury component to both CL/F and V/F produced significant improvement in the fitting (ΔAIC, −98). Figure 2 compares CWRES-versus-time diagnostic plots for the base model versus the final model. The apparent residual decrease in the base model diminished after accounting for time-dependent property in the final model (Figure 2B). The residual error was best described using a multiplicative error model. No noticeable trends indicating model misspecification were detected from the basic goodness-of-fit plots of the final model (Figure 3). The observed concentration-versus-population-predicted concentration plot (Figure 3A) showed that data were dispersed around the line of identity. The observed concentration-versus-

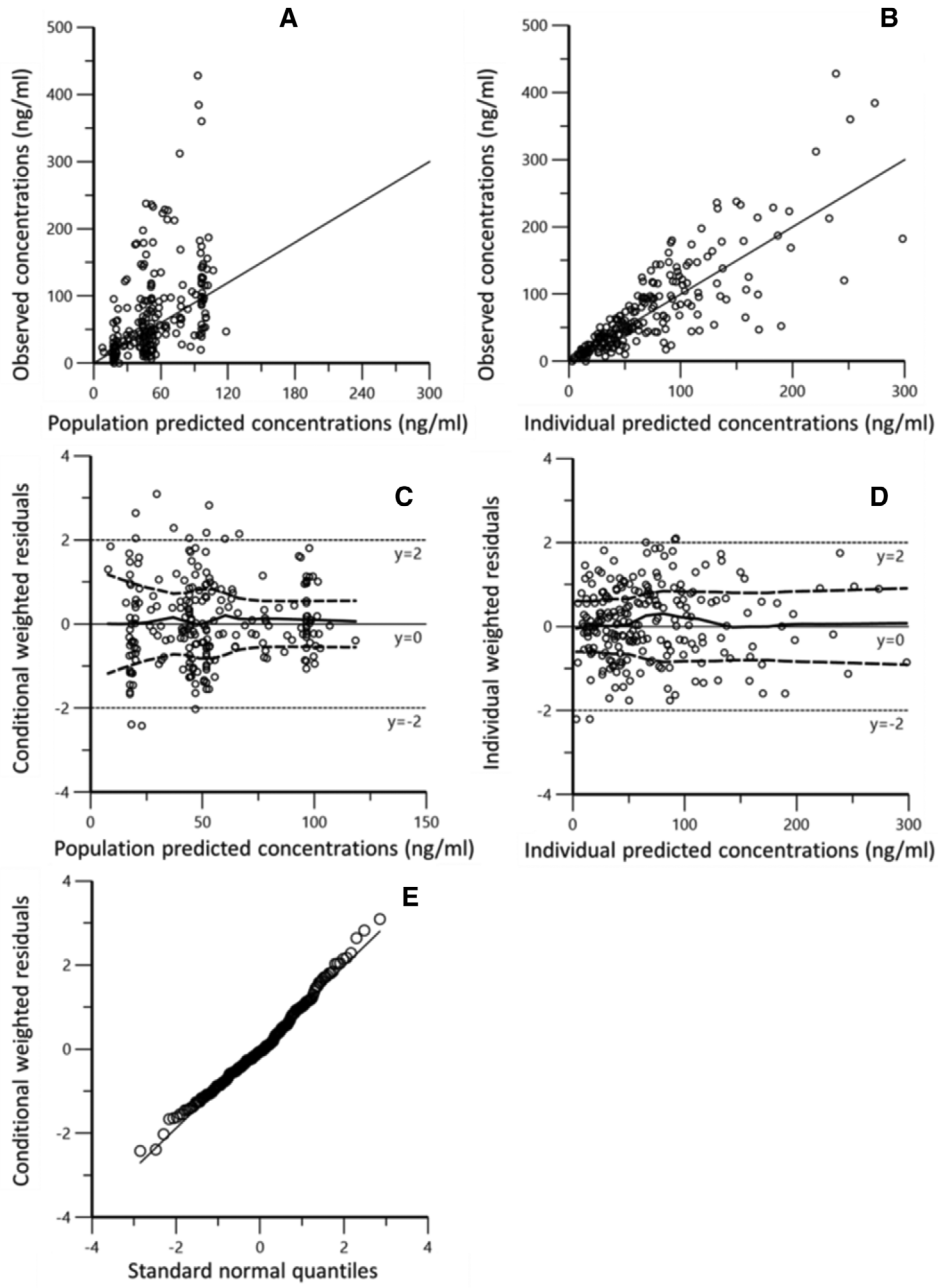

Figure 3. Visual pharmacokinetic model checks. Observed versus population-predicted concentrations (A) and versus individual-predicted concentrations (B). Conditional weighted residuals versus population-predicted concentrations (C). Individual weighted residuals versus individual predicted concentrations (D). Quantile-quantile plot of the components of conditional weighted residuals (E).

individual-predicted concentration plot (Figure 3B) revealed that data were scattered around the line of identify, indicating that the structural component was adequately fitted for most patients. The CWRES-versus-population-predicted plot (Figure 3C) demonstrated that residuals are evenly distributed about zero with a majority of the points falling within the 2-fold error boundaries, indicating no major misspecifications in the structural model, residual error model, or interindividual variability model. The individual-weighted residual-versus-individual predicted plot (Figure 3D) showed most points fall within 2-fold error, indicating no major bias in the error model or structural model. The quantile-quantile plot (Figure 3E) clarified that the components of conditional weighted residuals have no major deviation, confirming that the structural model is adequate. There was large shrinkage for k_a (99%), which was because of the incapability of capturing the absorption phase with the limited sampling times. Therefore, the

Table 2. Summary of Parameters of Riluzole From the Population PK Covariate Model

Parameters	Description	Estimates (CV%)	95%CI[b]	Shrinkage
k_a (h^{-1})	Absorption rate constant	5[a]		
CL/F (L/h)	Initial apparent clearance	38.8 (16.3%)	28.2-54.4	
I_{max_CL}	Maximum fold increase in clearance	4[a]		
t_{50_CL} (h)	Time at which half the increase in clearance is reached	800 (14%)	470-1572	
V/F (L)	Initial apparent volume of distribution	21.4 (15.3%)	14.8-36.0	
I_{max_V}	Maximum fold increase in volume of distribution	4[a]		
t_{50_V} (h)		7.89 (49.4%)	0.62-22.8	
CL/F IIV (%)		45.1 (10.5%)	22.2-67.5	5.3
V/F IIV (%)		42.9 (15.0%)	11.5-80.4	10.1
Covariance (CL,V)		41.6 (11.1%)	16.6-66.3	
Multiplicative residual error		0.454 (6.0%)	0.384-0.517	11.8
CL equation	$CL_{i,t/F} = \frac{CL}{F} \times \exp\left(\frac{Imax_{Cl} * Timei}{t50_{Cl} + Timei}\right) \times \exp(\eta CL_i)$			
V equation	$V_{i,t/F} = \frac{V}{F} \times \exp\left(\frac{Imax_V \times Timei}{t50_V + Timei}\right) \times \exp(\eta V_i)$			

[a] Fixed parameter.
[b] 95%CI is the 95th percentile confidence interval taken from a nonparametric bootstrap.

absorption constant was assumed to be the same on days 3, 7, 10, and 14 and fixed to 5/h, as previously established in the ALS population.[8,16] Omega shrinkage was low for CL/F and V_d/F (5.3% and 10.1%, respectively), suggesting that our data were sufficient to precisely estimate the individual parameters. The final PK parameters along with their unexplained interindividual variation (IIV) and the final equations describing apparent clearance and volume of distribution changes over time are summarized in Table 2. FOCE-ELS approach was employed to estimate baseline clearance (CL/F), and volume of distribution (V_d/F), which were 38.8 L/h, and 21.4 L, respectively. The increase in CL/F and V_d/F could both be described using the Michaelis Menten equation, featuring an increase over time that reaches a maximal change. Because t_{50} values are sensitive to changes in I_{max} for our given set of data, maximal increase (I_{max}) in CL and V was fixed to 4-fold to allow t_{50} to reflect the rate of change over time. The fixed values of both I_{max} (4) were determined by freezing I_{max_CL}, $I_{max}\_V_d$, t_{50}_CL, and $t_{50}\_V_d$ one term at a time to derive the value that most stabilized and optimized the estimation of the rest of the parameters. We also attempted to capture variability in the rate of change between patients by adding IIV components to t_{50} terms, but the variations could not be accurately captured, having high CV% and negative lower 2.5% confidence interval, indicative of model overparameterization. In the final model, smaller $t_{50}\_V_d$ compared with t_{50}_CL is indicative of a faster increase in apparent volume of distribution as compared with apparent clearance. The t_{50}_CL is estimated to be 800 hours, indicating a more gradual linear increase in clearance during the 14 days (336 hours) of riluzole treatment.

Serum albumin measured at baseline and on days 3, 7, 10, and 14 was explored as a potential covariate to explain the increased PK over 14 days. However, incorporating serum albumin did not improve the model fitting.

A visual predictive check was performed by simulating new data sets using the final model parameters (Figure 4). Prediction intervals (at 95%) constructed from simulated concentration-time profiles adequately captured the observed data.

Discussion

The population PK of riluzole has been studied in the context of ALS; however, the PK of riluzole patients with traumatic SCI has not been explored extensively. The altered time-varying PK of riluzole is a phenomenon only observed so far in the SCI population. Factors influencing absorption, metabolism, distribution, and elimination might not be the same among the inherently different neurological conditions, including ALS. Sex and smoking status contribute to the variations in riluzole exposure of ALS patients,[16] but played no role in the disposition of riluzole in SCI patients.[8] There may be sources of variation that do

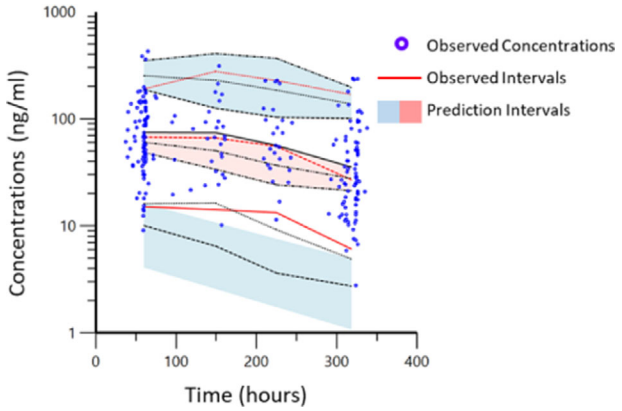

Figure 4. Visual predictive check of riluzole population pharmacokinetic model. Individual observations are presented by the blue dots. The 5th, 50th, and 95th percentiles of observed data are presented by the red lines. The 5th, 50th, and 95th percentiles of predicted data are presented by the black lines.

not exist in ALS contributed by SCI secondary injury mechanisms that arose during the subacute phase (48 hours to 14 days) postinjury. Therefore, the aim of this study was to characterize the PK of riluzole in the heterogeneous SCI population, accounting for the time-dependence property for maintaining the intended exposure over the 2-week treatment period in the future.

This analysis demonstrated that a 1-compartment PK model with time-varying CL/F and V_d/F adequately describes the concentration-time course of riluzole in patients with acute SCI. A Michaelis Menten function was adapted to reflect a maximal change in CL/F and V_d/F over the 14-day study period. This approach sufficiently captured the varying degree of increases in CL/F and V_d/F as SCI progresses postinjury.

Impact of SCI on Bioavailability

Although motor impairments may be the most obvious manifestation of SCI, the autonomic repercussions may be more catastrophic in comparison. Disruption of spinal autonomic pathways induces dysfunction or failure in multiple organs, manifesting as disordered cardiovascular, gastrointestinal, and renal function.[17] These autonomic dysfunctions can alter dispositions of therapeutics prescribed and/or tested in this heterogeneous population. The disruption of autonomic homeostasis may reduce absorption because of impaired gastric emptying, slow intestinal mobility, and reduced microvascular gastrointestinal blood flow.[18,19] In SCI patients, orally administrated drugs such as aspirin and paracetamol take a longer time to absorb and reach the peak concentration in plasma compared with uninjured controls.[20] The absorption process of riluzole may also be impaired, as the drug is taken orally in our study. Because of the feasibility of the study, sampling times are only taken at perceived peak and trough times, and therefore the absorption phase was not captured. Our model used a fixed k_a of riluzole, established from patients with ALS,[16] to construct PK profiles on days 3, 7, 10, and 14. This may or may not represent the true physiological phenomena, but the unaltered absorption process was assumed. In a study with SCI rats, the time course of SCI-induced disordered gastric emptying and motility showed that the conditions persist but do not vary for 6 weeks postinjury.[21] Therefore, it is not unreasonable to assume that the altered absorption of riluzole with SCI will not change further but remain relatively steady at the initial altered level post-SCI throughout the 2-week treatment period. In addition, the lower bioavailability because of the initial reduced absorption cannot explain the marked, continuous increases in F-normalized CL (CL/F) and V_d (V_d/F) from day 3 to day 14.

Impact of SCI on Apparent Clearance

The lower clearance of riluzole at the start of treatment compared with day 14 can be attributed to the decreased hepatic microvascular blood flow and hepatocyte gene expression immediately following the injury. Immediately following neurogenic shock, there is low circulation volume and low cardiac output, which contribute to the decreased microvascular blood flow in the liver, spleen, and skeletal muscle.[19,22] The reduction is likely from redirection of blood flow to maintain an adequate perfusion of the brain and heart.[23] Biotransformation of drugs depends on the amount of drug arriving in the liver and the expression of cytochrome P450, both of which require adequate hepatic blood flow. Consequently, reduced blood circulation into the liver will cause a decrease in the metabolism of drugs. Reports have shown that metabolism of high-extraction drugs such as phenacetin, methylprednisolone, and cyclosporine are lower in patients with SCI compared with able-bodied controls.[24–26] Riluzole has an intermediate hepatic extraction ratio, which subjects its metabolism to hepatic blood flow, protein binding, and intrinsic clearance. Therefore, impaired hepatic clearance shortly after injury may reduce riluzole metabolism in the liver and thus may only temporarily enhance its initial bioavailability in systemic circulation. Therefore, impaired hepatic clearance alone could not be adequately accounted for the observed continuous increases of CL/F and V_d/F from day 3 to day 14. The visual predictive check plot revealed an underprediction for lower concentrations, which may have come from a 1-compartment model being used instead of a 2-compartment model because of limited data points. A future study with intensive PK sampling in the SCI population would benefit resolving the identifiability issues with sparse sampling typically encountered in a challenging population.

Impaired renal function after SCI may cause a decrease in elimination of polar drug molecules, potentially accumulating to a toxic level,[27] as seen with ketamine, vancomycin, and lorazepam.[31–33] However, riluzole is excreted unchanged in urine at only 2% of the dose, and thus its urinary excretion may not be significantly affected by SCI.

Impact of SCI on Apparent Volume of Distribution

We initially speculated that the increase in riluzole volume distribution from day 3 to day 14 was because of the alterations in blood plasma constituents that drive blood-tissue partitioning. The plasma concentration of interleukin-2R is found to be significantly elevated in SCI individuals, reflecting a nonspecific immune response to system decentralization and autonomic perturbation.[28] Interleukin-2R induces albumin uptake by endothelial cells, which leads to the redistribution of albumin-rich intravascular fluid to extravascular sites.[29] Albumin is the main plasma protein that is responsible for drug transport. As a result of hypoalbuminemia, drugs with high protein binding will have increased distribution, whereas drugs with low protein binding will not be affected.[27] However, our analysis indicated that albumin level was not a significant covariate (unpublished data), suggesting that the increase in volume of distribution cannot be explained by albumin level alone, but rather by a collective sum of autonomic consequences. Young and Ensom found that the volume of distribution of aminoglycosides is significantly higher in the SCI population than the non-SCI population.[30] Other drugs with increased distribution have also been identified such as ketamine and lorazepam.[31,32] Similarly, the authors speculate that the smaller riluzole tissue distribution at the start of therapy that increased with time from day 3 to day 14 may be attributed, in part, to the expanded extracellular fluid volume characteristic of hyponatremia, a common electrolyte disorder during the acute stage post-SCI.[34] More data reflective of SCI progression are needed to improve the model fitting and explanation of the dynamic change in volume of distribution of riluzole PK.

The SCI population is heterogeneous and requires complex treatment regimens to alleviate comorbidities from secondary complications. SCI patients may take up to 21 concomitant medications during the acute phase for pain, spasticity, urinary tract infection, and pressure sores. The use of multiple medications by SCI patients increased their risk for drug-drug interactions. In future studies, we will evaluate the effects of concomitant medications that interfere with CYP1A2, a riluzole-metabolizing enzyme. In addition, riluzole is a substrate for P-glycoprotein (P-gp), a drug efflux transporter. P-gp is expressed in multiple tissues of the body, including the luminal membrane of capillary endothelial cells lining the blood-brain barrier, blood-spinal cord barrier, and gastrointestinal tract. Concurrent administration with any P-gp substrate/inhibitor/inducer may alter riluzole disposition. More recently, several studies have shown that in neurological diseases characterized by high excitotoxicity, oxidative stress, and inflammation in the brain, P-gp can become pathologically overexpressed at the blood-brain barrier, dramatically diminishing delivery of therapeutic drugs to the central nervous system.[35–37] Therefore, it is imperative to identify commonly coadministered medications in this cohort that pose a potential risk to alter riluzole PK. In addition, it would be beneficial and interesting to investigate whether other coadministered medications exhibit the same PK changes over the course of the treatment.

Although this study achieved our aims of characterizing the change in PK of riluzole over the treatment course, the absence of mechanistic information has to be noted as one of the limitations of the study. A secondary injury cascade is complex and affects multiple biological processes to varying degrees; as a result, the changing PK was not likely caused by a single factor. To further understand the effects of SCI on distribution, a biodistribution study repeated over time using an SCI animal model can shed light on exactly how partitioning into different organs changes as SCI progresses. In addition, measurement of the CYP1A2 enzyme over time can confirm our hypothesis that the reduced microvascular blood flow affecting intrinsic clearance of riluzole. Our study did not investigate active metabolites, which could potentially compensate for increased metabolism and maintain therapeutic levels of riluzole to preserve the intended efficacy. It will be feasible to fully evaluate the effects of time-dependent PK on neurological and behavioral recovery once the current trial concludes and the pharmacodynamic (PD) data are unblinded.

Development of effective treatment for SCI is challenging because of the substantial initial mechanical damage and subsequent destructive biochemical cascade. Understanding the PK and PD of therapeutics, as well as how disease progression can affect these properties, can facilitate drug development via an optimal dosing regimen design.

This study performed population PK modeling to describe, for the first time, the longitudinal impact of SCI-induced physiologic and molecular alterations on PK changes in riluzole. This model serves as a foundation to build a more elaborate model capable of personalized dosing as a function of time postinjury. Once the PK/PD relationship is established, the final model will have the potential to accurately predict patients' time-varying riluzole profiles and thus modify the regimen to maintain the optimal therapeutic levels

with minimal toxicity by taking into consideration a patient's characteristics, clinical course, and concurrent treatment for comorbidities. Going forward, additional PK studies in the SCI population may be warranted to enable the expansion of the developed PK model to address the longitudinal impact of SCI on other utilized drugs and potential drug-drug interactions, as well as the risks related to polypharmacy in this population.

Acknowledgments

The authors thank the patients and their families and the study coordinators and technicians for providing the clinical samples and patient data from the clinical trials. We also thank Susan Howley from the funding agency for her support to the authors, clinical investigators, and for preparation of this article.

Conflicts of Interest

The authors declare no conflicts of interest directly relevant to the content of this publication.

Funding

This study was supported by US ARMY MEDICAL RESEARCH ACQUISITION ACTIVITY under Contract No. W81XWH-16-C-0031.

Author Contributions

R.G.G., M.G.F., and D.S.C. designed the research. J.S.H., K.M.S., M.M.J., J.D.G., B.A., C.I.S., M.B., and R.F.F. recruited patients and conducted the clinical research. E.G.T. provided operational oversight and regulatory compliance. A.N. developed the manuscript with comprehensive pharmacokinetic analysis and modeling. L.W. provided modeling support. A.N., Y.T., and M.S. analyzed the phase 1 data.

The data cannot be shared at this moment because of the confidentiality of the ongoing clinical trial.

References

1. National Spinal Cord Injury Statistical Center. *Facts and Figures at a Glance*. Birmingham, AL: University of Alabama at Birmingham; 2020.
2. Ahuja CS, Wilson JR, Nori S, et al. Traumatic spinal cord injury. *Nat Rev Dis Prim*. 2017;3:17018.
3. Bensimon G, Lacomblez L, Meininger V. A controlled trial of riluzole in amyotrophic lateral sclerosis. *N Engl J Med*. 1994;330(9):585-591.
4. Lacomblez L, Bensimon G, Meininger V, Leigh PN, Guillet P. Dose-ranging study of riluzole in amyotrophic lateral sclerosis. *The Lancet*. 1996;347 (9013):1425–1431.
5. Doble A. The pharmacology and mechanism of action of riluzole. *Neurology*. 1996;47 (6 suppl 4):233S–241S.
6. Ates O, Cayli SR, Gurses I, et al. Comparative neuroprotective effect of sodium channel blockers after experimental spinal cord injury. *J Clin Neurosci*. 2007;14(7):658-665.
7. Le Liboux A, Lefebvre P, Le Roux Y, et al. Single- and multiple-dose pharmacokinetics of riluzole subjects in white subjects. *J Clin Pharmacol*. 1997;37(9):820-827.
8. Chow DSL, Teng Y, Toups EG, et al. Pharmacology of riluzole in acute spinal cord injury. *J Neurosurg Spine*. 2012;17:129-140.
9. Fehlings MG, Nakashima H, Nagoshi N, Chow DSL, Grossman RG, Kopjar B. Rationale, design and critical end points for the Riluzole in Acute Spinal Cord Injury Study (RISCIS): A randomized, double-blinded, placebo-controlled parallel multicenter trial. *Spinal Cord*. 2016;54(1):8-15.
10. Sarkar M, Grossman RG, Toups EG, Chow DSL. UPLC–MS/MS assay of riluzole in human plasma and cerebrospinal fluid (CSF): Application in samples from spinal cord injured patients. *J Pharm Biomed Anal*. 2017;146:334-340.
11. Liu C, Yu J, Li H, et al. Association of time-varying clearance of nivolumab with disease dynamics and its implications on exposure response analysis. *Clin Pharmacol Ther*. 2017;101(5):657-666.
12. Wilkins JJ, Brockhaus B, Dai H, et al. Time-varying clearance and impact of disease state on the pharmacokinetics of avelumab in merkel cell carcinoma and urothelial carcinoma. *CPT Pharmacometrics Syst Pharmacol*. 2019;8(6):415-427.
13. Gibiansky E, Gibiansky L, Carlile DJ, Jamois C, Buchheit V, Frey N. Population pharmacokinetics of obinutuzumab (GA101) in chronic lymphocytic leukemia (CLL) and non-Hodgkin's lymphoma and exposure-response in CLL. *CPT Pharmacometrics Syst Pharmacol*. 2014;3(10):1-11.
14. An G. Concept of pharmacologic target-mediated drug disposition in large-molecule and small-molecule compounds. *J Clin Pharmacol*. 2020;60(2):149-163.
15. Würthwein G, Lanvers-Kaminsky C, Hempel G, et al. Population pharmacokinetics to model the time-varying clearance of the PEGylated asparaginase Oncaspar® in children with acute lymphoblastic leukemia. *Eur J Drug Metab Pharmacokinet*. 2017;42(6):955-963.
16. Bruno R, Vivier N, Montay G, et al. Population pharmacokinetics of riluzole in patients with amyotrophic lateral sclerosis. *Clin Pharmacol Ther*. 1997;62(5):518-526.
17. Taylor JA. Autonomic consequences of spinal cord injury. *Auton Neurosci Basic Clin*. 2018;209:1-3.
18. Fealey RD, Szurszewski JH, Merritt JL, DiMagno EP. Effect of traumatic spinal cord transection on human upper gastrointestinal motility and gastric emptying. *Gastroenterology*. 1984;87(1):69-75.
19. Guízar-Sahagún G, Velasco-Hernández L, Martínez-Cruz A, et al. Systemic microcirculation after complete high and low thoracic spinal cord section in rats. *J Neurotrauma*. 2004;21(11):1614-1623.
20. Fuentes-Lara G, Guízar-Sahagún G, García-López P. Effect of experimental spinal cord injury on salicylate bioavailability after oral aspirin administration. *J Pharmacol Toxicol Methods*. 1999;42(2):93-97.
21. Holmes GM, Blanke EN. Gastrointestinal dysfunction after spinal cord injury. *Exp Neurol*. 2019;320(March):113009.
22. Seifert J, Lob G, Probst J, Brendel W. Microcirculation and blood volume in rats before and after spinal cord injury. *Paraplegia*. 1979;17(4):436-440.
23. Cruz-Antonio L, Flores-Murrieta FJ, García-Löpez P, Guízar-Sahagún G, Castañeda-Hernández G. Understanding drug disposition alterations induced by acute spinal cord injury: Role of injury level and route of administration for agents submitted to extensive liver metabolism. *J Neurotrauma*. 2006;23(1):75-85.
24. Vertiz-Hernandez A, Castaneda-Hernandez G, Martinez-Cruz A, Cruz-Antonio L, Grijalva I, Guizar-Sahagun G. L-arginine reverses alterations in drug disposition induced by spinal

cord injury by increasing hepatic blood flow. *J Neurotrauma*. 2007;24(12):1855-1862.
25. Segal JL, Maltby BF, Langdorf MI, Jacobson R, Brunnemann SR, Jusko WJ. Methylprednisolone disposition kinetics in patients with acute spinal cord injury. *Pharmacotherapy*. 1998;18(1):16-22.
26. García-López P, Martínez-Cruz A, Guízar-Sahagún G, Castãeda-Hernández G. Acute spinal cord injury changes the disposition of some, but not all drugs given intravenously. *Spinal Cord*. 2007;45(9):603-608.
27. Mestre H, Alkon T, Salazar S, Ibarra A. Spinal cord injury sequelae alter drug pharmacokinetics: An overview. *Spinal Cord*. 2011;49(9):955-960.
28. Segal JL, Gonzalez E, Yousefi S, Jamshidipour L, Brunnemann SR. Circulating levels of IL-2R, ICAM-1, and IL-6 in spinal cord injuries. *Arch Phys Med Rehabil*. 1997;78(1):44-47.
29. Zloza A, Kim DW, Broucek J, Schenkel JM, Kaufman HL. High-dose IL-2 induces rapid albumin uptake by endothelial cells through Src-dependent caveolae-mediated endocytosis. *J Interferon Cytokine Res*. 2014;34(11):915-919.
30. Young F, Ensom MHH. Pharmacokinetics of aminoglycosides in patients with chronic spinal cord injury. *Am J Heal Pharm*. 2011;68(17):1607-1614.
31. Hijazi Y, Bodonian C, Bolon M, Salord F, Boulieu R. Pharmacokinetics and haemodynamics of ketamine in intensive care patients with brain or spinal cord injury. *Br J Anaesth*. 2003;90(2):155-160.
32. Segal JL, Brunnemann SR, Eltorai IM, Vulpe M. Decreased systemic clearance of lorazepam in humans with spinal cord injury. *J Clin Pharmacol*. 1991;31(7):651-656.
33. Lavezo LA, Davis RL. Vancomycin pharmacokinetics in spinal cord injured patients: a comparison with age-matched, able-bodied controls. *J Spinal Cord Med*. 1995;18(4):233-235.
34. Furlan JC, Fehlings MG. Hyponatremia in the acute stage after traumatic cervical spinal cord injury: Clinical and neuroanatomic evidence for autonomic dysfunction. *Spine (Phila Pa 1976)*. 2009;34(5):501-511.
35. Dulin JN, Moore ML, Grill RJ. The dual cyclooxygenase/5-lipoxygenase inhibitor licofelone attenuates P-glycoprotein-mediated drug resistance in the injured spinal cord. *J Neurotrauma*. 2013;30(3):211-226.
36. Milane A, Fernandez C, Dupuis L, et al. P-glycoprotein expression and function are increased in an animal model of amyotrophic lateral sclerosis. *Neurosci Lett*. 2010;472(3):166-170.
37. Qosa H, Lichter J, Sarlo M, et al. Astrocytes drive upregulation of the multidrug resistance transporter ABCB1 (P-glycoprotein) in endothelial cells of the blood–brain barrier in mutant superoxide dismutase 1-linked amyotrophic lateral sclerosis. *Glia*. 2016;64(8):1298-1313.